J Forensic Sci, Jan. 2005, Vol. 50, No. 1
Paper ID JFS2004268
Available online at: www.astm.org

L. Scott Chumbley,[1] *Ph.D. and Fran C. Laabs,*[1] *M.S.*

Analysis of Explosive Damage in Metals Using Orientation Imaging Microscopy*

ABSTRACT: The goal of this project was to determine whether quantitative information concerning the size and nature of an explosive blast could be determined using Orientation Imaging Microscopy (OIM) to analyze the texture of blast-affected metal. Selected 1018 steel and 2024 aluminum samples were subjected to various explosive blasts chosen to simulate a wide range of possible pressure waves. The explosives used were PBX 9404, Comp-C4, Gelmax, and Bullseye. The explosive tests were carried out at Sandia National Laboratory, and the OIM analysis was conducted at Ames Laboratory. It was discovered that while suitable patterns could be obtained from the steel samples, the oxide layer present on the surface of the aluminum samples prevented these samples from being studied. The results of the OIM studies on the steel samples indicate that damage can be tracked using OIM imaging and that Comp-C4 seems to produce patterns significantly different than the other explosives.

KEYWORDS: forensic science, orientation imaging microscopy, explosive damage, pressure wave, texture

With the rise of terrorist activities has come an increased desire to develop new methods to characterize the effects of explosive blasts. What is desired is a characterization method that is fairly simple to use, involves little sample preparation, and can be easily understood by untrained personnel. Ideally the method would provide some type of quantitative assessment of the force of the blast to assist in identification as well as a visual representation for qualitative assessment.

Numerous studies have been conducted on the effects of shock-induced damage (1,2). Methods to produce the loading include explosive forces (3,4) and high pressure guns (5). Several studies have employed transmission electron microscopy to examine the microstructure of various materials subjected to high-pressure shock waves (6,7). These studies have shown that in some materials the dislocation structure that develops as a result of the shock wave is similar to what is produced in materials that have been deformed more slowly by conventional mechanical deformation methods (8). Other studies show that some dislocation substructures and twins are unique to given materials when subjected to explosive blasts, e.g., some twinning in aluminum alloys used in aircraft structures and characteristic phase formation (9,10). While these studies and others (11–13) have extensively examined the dislocation substructure on a microscopic scale, they did not attempt to evaluate on a macroscopic scale the degree to which any initial texture may have been influenced by the shock wave.

Orientation Imaging Microscopy (OIM) uses the electron backscattering signal to examine the matrix of the metal to detect the crystallographic orientation (14). The technique does not require extensive sample preparation, and only a relatively small amount of material is required. The technique can produce qualitative visual, as well as quantitative data. As such, it is an interesting method to use to see if textual differences produced due to varying pressure waves could be identified.

This study involved the examination of various metal samples exposed to shock waves produced by explosive detonations. Since the pressure of an explosive blast drops off by two orders of magnitude if an air gap exists between the explosive and the metal, the most dramatic deformation effects should be seen for explosives in contact with the test piece. In this study a selection of detonations was examined to see if OIM could be used to deduce the pressure wave type and amplitude. Although this will not yield an unambiguous answer as to the explosive type, it should be possible to place it in a range of explosives.

Experimental Procedure

Samples known as "dent tests" were provided by Sandia National Laboratory, Table 1. Four different explosives were used, namely, PBX9404, C4 plastic explosive, Gelmax dynamite, and Bullseye gunpowder. The explosives were loaded into cardboard cylinders and placed on top of the metallic materials. Two different materials were examined, a common 1018 steel and 2024 aluminum in the T-6 heat treatment state. The steel samples were square blocks, 4 in × 4 in. and 1 in. thick, while the aluminum samples were square blocks 6 in. × 6 in. by 3 in. thick. The sizes were chosen such that the entire force of the explosion (and subsequent deformation) would remain within the material without through-penetration of the block by the blast. The control samples for each series were labeled sample 1, while the individual shots were labeled samples 2–4, with a letter designation giving the type of explosive used. From this matrix of test samples individual shots were selected, sectioned, and examined using OIM. The shock pressure in each of the metal samples was calculated, and these values are shown in Table 2.

A typical shot would be sectioned for OIM examination in the following manner. A 3/16 in. cross sectional slice was first obtained through the blast dent, then smaller samples, hereafter referred to as coupons, were removed from various locations using a low-speed diamond saw. In the initial study of the steel sample, the

[1] US DOE Ames Laboratory.

* This work was funded by the Federal Bureau of Investigation, Dean Federoff, Contract Manager, performed in part at Ames Laboratory under contract No. W-7405-Eng-82 with the US Department of Energy. This work has not been presented.

Received 3 July 2004; and in revised form 15 September 2004; accepted 15 September 2004; published 8 Dec. 2004.

TABLE 1—*Test matrix of samples.*

	Explosive			
Metal	A. PBX9404 1″ dia. × 4″	B. Comp-C4 1.2″ dia. × 4.75″	C. Atlas Gelmax Dynamite 1.2″ dia. × 4.75″	D. Hercules Bullseye Gunpowder 1.2″ dia. × 4.75″
Steel (1018)	1 = control A2-4 = test shots	B2-4 = test shots	C2-4 = test shots	D2-4 = test shots
Aluminum (2024-T6)	1 = control A2-4 = test shots	B2-4 = test shots	C2-4 = test shots	D2-4 = test shots

TABLE 2—*Pressure in target samples.*

	Pressure in Target Metal (GPa)	
Explosive	2024 Aluminum	1018 Steel
(A) PBX9404	42.4	58.3
(B) Comp-C4	33.3	44.2
(C) Gelmax	5.95	7.06
(D) Bullseye	5.67	6.42

as-received material was sectioned using a mechanical saw and electro-discharge machining to see if any difference in image quality was introduced during the initial sectioning. Since these samples looked essentially identical, all further samples were sectioned using the faster cut-off saw.

Sample locations were selected to give a range of pressure values away from the blast in various directions. Sectioning is illustrated in Fig. 1. Each coupon was examined in three orthogonal views to determine which coupons and directions would provide the best OIM information. Later investigations concentrated only on those areas that provided the most useful information. The samples were mechanically polished using an automatic polisher and diamond paste and lightly etched using Nital to remove the remaining effects of the polishing.

No successful method was found to polish the aluminum samples. The amorphous film that formed rapidly on the surface of Al either blurred or totally obscured the OIM patterns. This was unexpected since preliminary runs on Al foil where no polishing was used resulted in classic patterns and expected results. It appears that each Al alloy must be polished on an individual basis to determine the best method for reducing the oxide scale in that particular alloy. Due to the poor Al polishing results all further OIM efforts were concentrated on the steel samples. No Al data was obtained. This was unfortunate since this prevented any OIM comparison between blast effects on a body-centered cubic crystal structure (BCC) of steel with those on the face-centered cubic crystal structure (FCC) of Al.

OIM Parameters

All samples were examined using an Amray 1845 field emission scanning electron microscope equipped with a TSL orientation imaging system. The specimens were tilted at 70° from horizontal (30° angle between beam and specimen surface) and observed with a beam voltage of Eo = 25 KV, sample current = ~1 na. Typical step size was 3 μm, selected to give at least 10 samplings per grain. The examined area typically was in the range of 400–600 × 800–1000 μm depending on grain size and available time.

Experimental Results

The type of data obtained for each set consists of the images and the quantitative numerical values assigned for a number of different methods of describing the sample's crystallographic texture. Representative OIM images will be shown to provide a general overview of the types of images obtained after which the quantitative data will be discussed. Due to the large amount of data and images collected it would take several volumes to show all of the images while the numerical values can be averaged and summarized in one convenient table. These data are presented in Table 3. The different methods by which the crystallographic data is presented are described below. It is important to remember that each value is directly related to a graphic representation depicting the

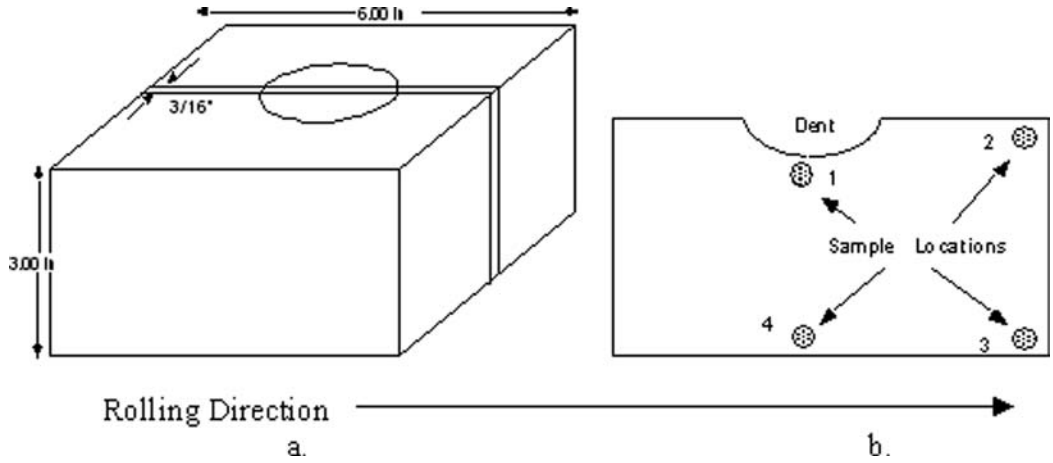

FIG. 1—*Example showing sectioning of a test piece: a) Schematic of the sample showing sectioning slice, b) Cross-sectioned slice showing location and labeling of the samples for OIM. The rolling direction of both schematics would be left to right.*

TABLE 3—*Summary of OIM data obtained from all samples.*

ID	Max PF		Max IPF		IQ		CI		Gr/Sze
	max	min	max	min	Max	Ave	Max	Ave	Ave
As-received 1018 Steel									
Mechanically Cut									
V1	1.85	0.48	1.74	0.17	134.8	80	0.971	0.339	60
V2	1.67	0.5	1.48	0.16	133.5	76.6	0.970	0.343	60.3
V3	2.52	0.8	1.76	0.92	125.3	81	0.950	0.481	84.9
V3b	1.78	0.48	1.46	0.21	96.3	49.6	0.970	0.509	123
Electro-Discharge									
V1	2.07	0.43	1.48	0.18	88.3	48.97	0.971	0.403	73.8
V2	2.01	0.46	1.51	0.26	66.3	37.5	1.000	0.300	165
V3	1.83	0.35	1.61	0.23	76.4	41.1	1.000	0.338	56.4
PBX 9404 (Sample A)									
Coupon 1									
V1	5.96	0.22	5.56	0.4	79.5	11.19	1.000	0.090	22.2
V2b	3.44	0.29	1.49	0.21	47.3	15.5	1.000	0.147	16.8
V3	2.2	0.39	2.11	0.18	76.2	31.51	1.000	0.411	52.5
Coupon 2									
V1	2.41	0.41	1.75	0.17	65.4	24	1.000	0.220	24.9
V2	1.92	0.4	1.84	0.22	88.3	48.4	1.000	0.499	98.1
V2b	1.5	0.4	1.84	0.22	47.3	15.5	1.000	0.147	16.8
V3	2.96	0.42	4.06	0.24	72.6	37.8	1.000	0.464	70.8
Coupon 3									
V1	2.4	0.56	1.64	0.19	85.1	45.79	1.100	0.443	75
V2	1.78	0.56	1.55	0.22	79.9	43.65	0.971	0.315	56.1
V3	1.71	0.47	1.51	0.96	80.3	43.13	1.000	0.529	103
Coupon 4									
V1	2.01	0.28	1.88	0.15	69.8	35.8	1.000	0.461	85.2
V2	2.62	0.37	2.33	0.36	106.7	40.2	1.000	0.478	79.5
V3	2.15	0.39	1.71	0.92	65.8	25.5	1.000	0.327	36.0
Composition C4 (Sample B)									
Coupon 1									
V1	8.91	0.19	3.31	0.1	63.6	20.3	1.000	0.076	12.3
V1b	7.17	0.06	4.02	0.02	87.6	23.85	1.000	0.029	9.3
V2	4.37	0.25	3.2	0.13	46	10.75	1.000	0.078	15.3
V3	5.08	0.22	3.65	0.23	42.3	10.45	1.000	0.098	21
Coupon 4									
V1b	6	0.25	1.64	0	52.1	19.6	1.000	0.550	10.2
V2	3.58	0.24	1.72	0.18	48.7	25.98	1.000	0.295	36.6
V3	4.11	0.35	2.14	0.26	44.9	23.21	1.000	0.197	28.5
Gelmax Dynamite (Sample C)									
Coupon 1									
V1	1.97	0.39	1.66	0.21	64	30.72	1.000	0.448	76.5
V2b	1.7	0.43	1.45	0.96	96.3	51.87	1.000	0.521	96
V3	1.93	0.37	1.74	0.29	48.2	29.32	1.000	0.503	102.9
Coupon 4									
V1	1.74	0.45	1.55	0.21	62.5	35.45	1.000	0.575	99
V2	1.61	0.41	1.43	0.28	76.2	40.3	1.000	0.549	90.6
V3	1.89	0.54	1.46	0.22	48.3	29.61	1.000	0.524	93
Bullseye Black Powder (Sample D)									
Coupon 1									
V1	1.78	0.44	1.45	0.18	61.3	33.73	1.000	0.512	87.9
V2	2.43	0.3	2.55	0.27	45.2	14.08	1.000	0.182	39.9
V3	2.50	0.36	1.72	0.92	46.3	26.7	1.000	0.43	99.6
Coupon 4									
V1	1.66	0.49	1.47	0.23	64.1	37.79	1.000	0.549	95.7
V2	2.15	0.25	2.15	0.21	48.7	25.251	1.000	0.428	74.1
V3	4.12	0.47	1.91	0.24	46.3	27.66	0.971	0.319	46.5

crystallographic alignment of the grains.

- Pole Figure (Max PF)—This is a measure of how intense the alignment of the grains are as related to a stereographic projection.
- Inverse Pole Figure (Max IPF)—Describes the alignment of various crystallographic directions in the crystal with respect to the physical x, y, and z coordinates of the sample. X, y, and z are user defined to correspond to physical directions on the sample, e.g., the rolling direction, a wire direction, etc. Inverse pole figures, since they show more than one crystallographic direction in relation to the physical sample, can reveal multiple textures in the sample as well as the relative strengths of those textures.

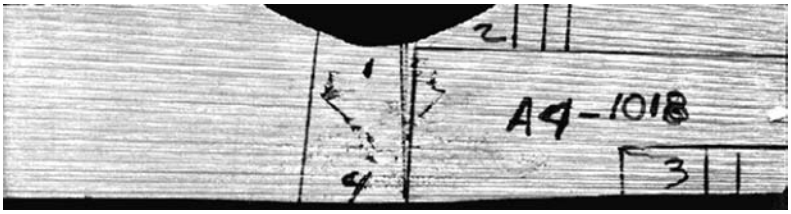

FIG. 2—*Example of cross-sectioned sample A4-1018 steel. The numbers and various lines indicate regions were coupons were to be cut. Note that Coupon 1 is directly below the dent, coupon 4 directly below but at a distance.*

- Image Quality (IQ)—A measure of how well the computer can recognize a pattern. This can be used to determine grain size and boundaries.
- Confidence Index (CI)—Measure of how well the computer was able to fit the data to a crystallographic direction. Higher numbers are better.
- Grain Size (Gr/Sze)—This is simply the grain size as measured by the computer.

Dent Test Samples

A typical image of a dent test sample cut shown in cross section is shown in Fig. 2. From a slice such as this, sample coupons were taken and then analyzed in three orthogonal directions to determine which sample location and which directions best revealed the blast damage.

The damage obtained from the dent tests was often extreme, giving OIM images where the confidence of matching was very low. This, in turn, resulted in tiled images that clearly displayed the disruption of the atomic stacking in the material. Since the tiled images reflected the damage in the material, these are shown in the following sections.

Control Sample

The initial image obtained from the control sample is shown in Fig. 3. A relatively random array of grains is seen, although evidence of the initial rolling texture can be detected in the structure. This is apparent by the alignment and elongation of the grain structure. Some slight residual damage from either polishing or handling also appears as an increase in the black areas that can be seen near the top of the figure. This image should now be compared to the images of Figs. 4–7. In each case the structure changes drastically after being subjected to the explosive force.

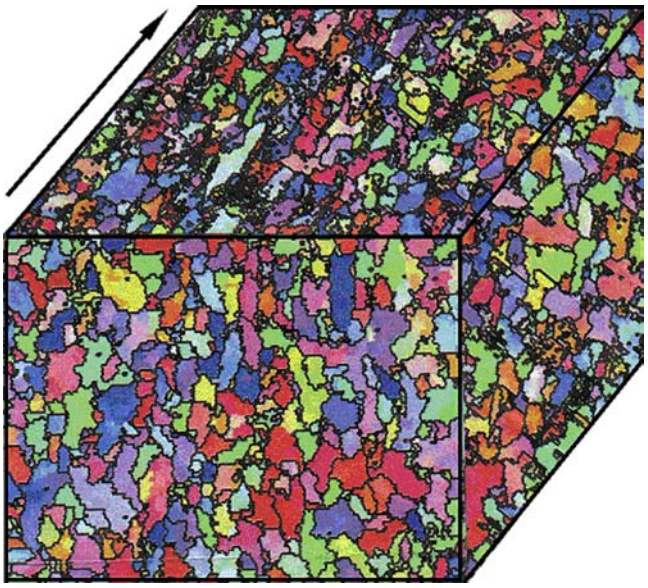

FIG. 3—*Tiled image showing orientation of as-received 1018 steel plate. The arrow shows the rolling direction of the original plate.*

PBX Sample A

Figure 4 shows a series of tiled images taken from the 1018 steel sample after it had been exposed to a blast from PBX explosive. Each tiled image represents the OIM data obtained from three orthogonal directions for each coupon. A great deal of time was spent on this sample since at the beginning of the study there were no data on the effect of explosive blasts on the quality of OIM images. Therefore, four sample coupons were examined for sample A, while only two were examined for the remaining three explosives. The tiled images from Coupons 1–4 are displayed in Fig. 4. Coupon 4 is displayed as Fig. 4*c* instead of 4*d* because this enables it to be placed directly under the tiled images for Coupon 1. By choosing to display the coupon in this manner, it is shown in the same physical arrangement as was present in the actual sample piece. (See Fig. 1. Coupons were labeled in a clockwise manner, starting from Coupon 1, directly below the blast.) Several interesting observations can be made based on Fig. 4:

- Within each coupon a large directionality effect is seen in the damage induced in the OIM images. For example, in Coupon 1 (Fig. 4*a*) top and bottom sides show extreme damage while the face shows a lower level of damage.
- As the location of the coupon gets further from the blast, the amount of damage generally decreases, as expected.
- In regions of heaviest damage the images show a slight preference in orientation to ⟨111⟩, the close-packed direction of the body-centered cubic steel crystal structure. This is indicated by the predominance of blue-tinted grains evident on the top and side of the image in Fig. 4*a*. This might indicate that texturing of the sample has occurred or that the ⟨111⟩ orientation grains were favorably oriented to withstand the movement of the shockwave through the material with little effect.
- In the heavily damaged material few grains are discernable. This illustrates that the problem with using grain size data as a measure of damage since the black regions are not counted in the grain size numbers.
- Even in the coupons and views furthest from the blast, evidence of shear bands can be observed in the microstructure.

The tabulated quantitative values of the dent test data are shown in Table 3. These values confirm the qualitative views presented in Fig. 4. (In this table, some runs were executed twice due to hardware problems or power outages. The aborted runs are not taken into account in the calculated averages.) Considering the pole figure number, an increase in value is seen. Note that by observation of Fig. 4 we see that the increase is not due to all

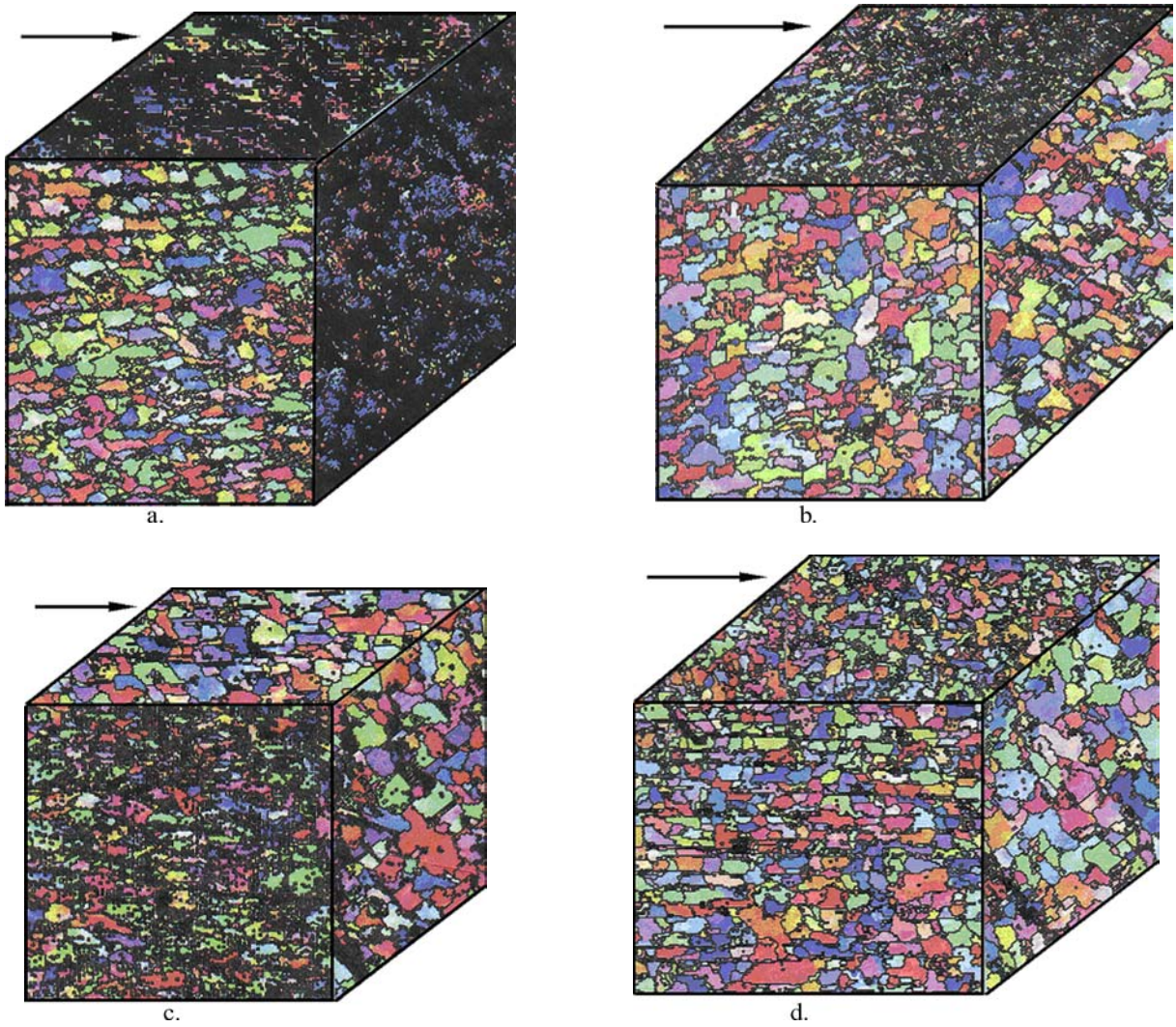

FIG. 4—*Tiled images of PBX Sample A, Coupons 1–4: a) Coupon 1, b) Coupon 2, c) Coupon 4, d) Coupon 3. Rolling direction as indicated.*

the grains becoming aligned, as Fig. 4 shows heavy damage preventing identification. Rather, the grains that can be recognized and plotted by the computer (the blue grains) are aligned along ⟨111⟩, either as a result of the blast or by being favorably disposed along this direction from their initial state. Both the image quality and the confidence index numbers agree with Fig. 4, being lower than the control samples, but increasing in value as damage decreases.

Two final points should be noted relating to the data of Table 3. First, two control samples are shown, one cut using mechanical methods and one cut using electro-discharge machining as a comparison. In all cases the EDM sample exhibited poorer quality patterns so the comparisons stated above and subsequently are made with respect to the mechanically cut sample. Secondly, since observation showed that most of the damage was concentrated in Coupons 1 and 4, only these views were examined in the remaining samples.

Comp-C4 Sample B

The tiled images for Coupons 1 and 4 for this sample, with three orthogonal views being shown, are displayed in Fig. 5. The C-4 dent tests produced the most distinctive images of any samples studied, in regards to both the amount of damage and the effect on the grain structure. A summary of observation on this sample is given below:

- The C-4 samples showed much more damage than the other samples. This is despite the fact that the calculated pressure wave for this sample is *lower* than what was experienced in the PBX sample.
- The appearance of the damage also varies considerably. Where grains could be identified by the computer, the large grained structure seen in the starting material was largely replaced by smaller grains in areas near the blast site. No other samples exhibited this structure.
- Where texturing has occurred (or results due to grains remaining after the blast), the observed texture is again ⟨111⟩, similar to the PBX sample.
- The "1" views (the front square faces of the images in Fig. 5) appear much different than the two remaining orthogonal views.

The C-4 dent tests seem to be anomalous among the samples studied. The results also appear to be repeatable, as the tiled images of repeat scans proved similar to the image displayed in Fig. 5. What is especially interesting is the appearance of the face of the tiled

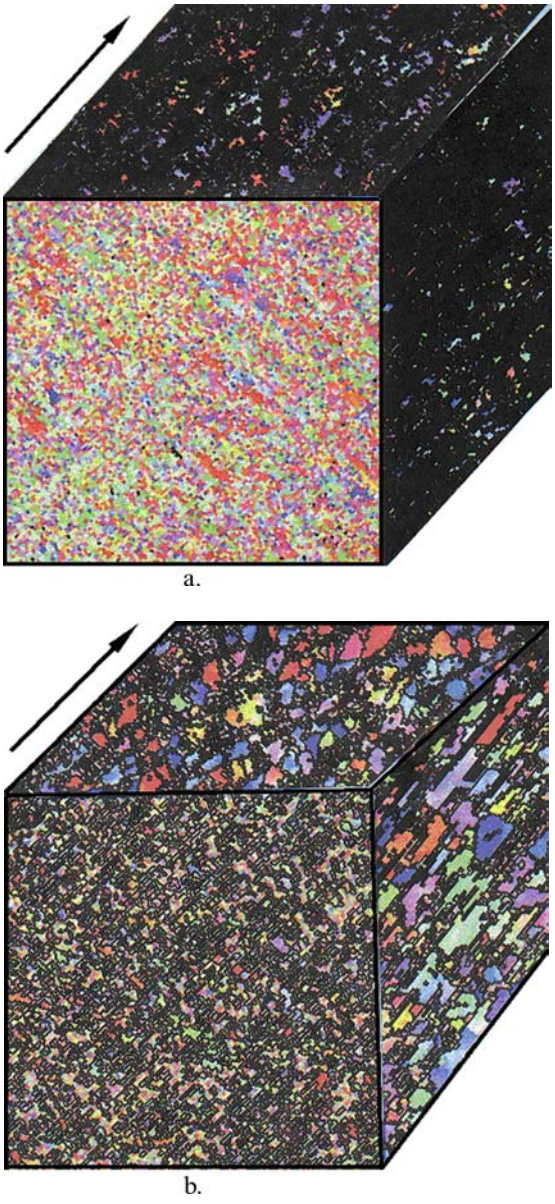

FIG. 5—*Tiled images of Comp C-4 Sample B, Coupons 1 and 4: a) Coupon 1, b) Coupon 4. Note that the "1" views correspond to the front faces of the images.*

image (the "1" view). Coupon 1, view 1 shows a high degree of grain refinement without a large amount of damage, although the other two views show severe damage. In Coupon 4 the "1" view shows a large amount of damage, but the fine grain structure is still discernable, while the other views simply show the original large grained structure with a significant amount of damage, including shear bands, similar to the damage seen due to the less robust explosive of Gelmax Dynamite described below. It appears that unlike the other samples the pressure wave from the Comp C-4 is causing high damage that, in certain directions, leads to a possible recrystallization of the damaged material into a new, fine-grained microstructure. Although we have mentioned the danger concerning using the grain size data as an absolute comparison between samples, it is interesting that the apparent grain size in the series C-4 samples is much lower than either the control or any of the other dent test samples. These findings need to be verified and tested again, but at this time it appears that C-4 explosions might be characterized on the basis of their OIM images.

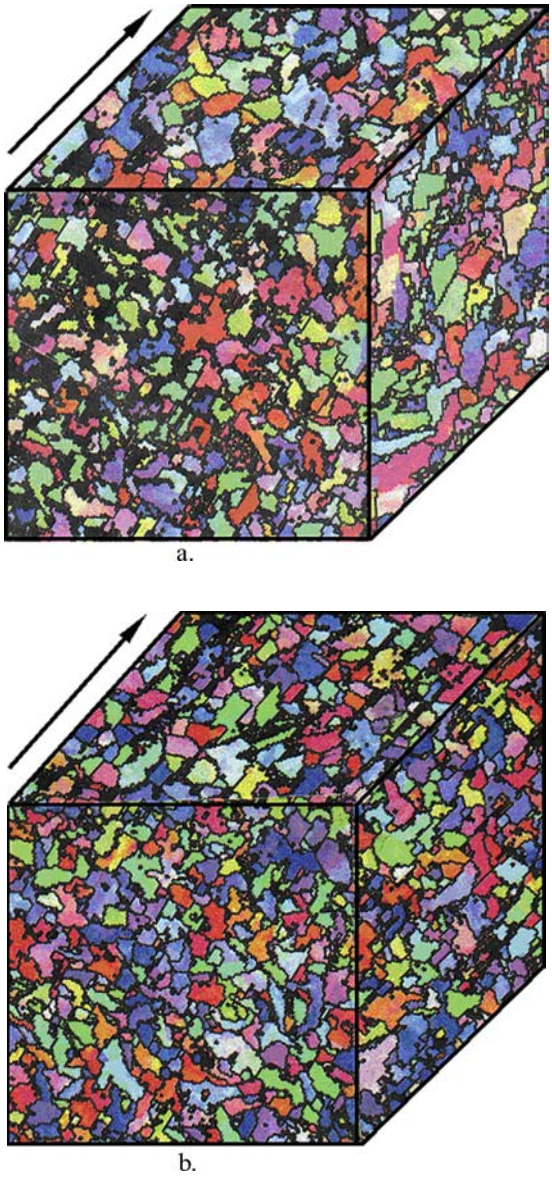

FIG. 6—*Tiled images of Gelmax Dynamite Sample C, Coupons 1 and 4: a) Coupon 1, b) Coupon 4.*

Gelmax Dynamite Sample C

The tiled images from Sample C are shown in Fig. 6. By comparison to the previous two samples it can be seen that damage in this series is relatively light. Damage generally appears as regions distributed throughout the grain structure of the material.

The appearance of the damage in this sample (and the D series samples, below) does suggest possible explanations for the texturing effects noted in the A and B series views. It appears that when visible damage begins to occur in the OIM images, it manifests itself as a disruption of the present grain structure to the extent that the computer can no longer recognize the crystal orientation. It does not appear to result in the rotation of grains. Viewing the A, C, and D series it also does not appear to result in the heating of the sample to the extent that a new grain structure appears. The possible exception to this is, of course, the comp-C4 samples of series B discussed earlier where a fine-grained structure is observed. Instead, it seems that damage accumulates with increasing pressure wave force, obliterating old grains instead of creating new ones with favorable orientation. Thus, the slight texture increase seen in the

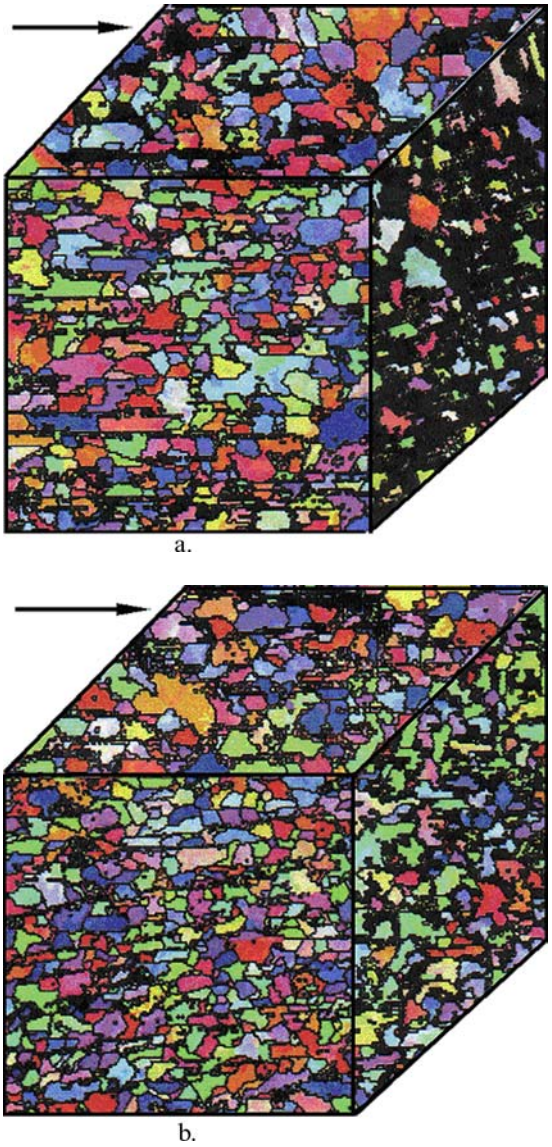

FIG. 7—*Tiled images of Bullseye Black Powder Sample D, Coupons 1 and 4: a) Coupon 1, b) Coupon 4.*

samples is due to existing favorably oriented grains withstanding the pressure wave relatively unchanged, rather than being formed as a result of the blast.

Bullseye Black Powder Sample D

The final sample examined was the sample subjected to a blast initiated using Bullseye black powder. The tiled images from this dent test are shown in Fig. 7. As for the C series, little damage is evident in the samples. Given these results it appears OIM characterization of low order explosions is difficult at best. It might be possible to obtain meaningful data in special circumstances where samples of the actual material both before and after the blast are available. However, as Fig. 7 shows, the damage from a low order blast appears very similar to residual stress that may be present in the starting material. While the amount of damage seems higher, it is impossible to tell whether the banding in the structure is due to the blast or is just left from the initial rolling of the material. (See Fig. 3 for a comparison of the damage due to rolling of the sheet.) Thus, OIM imaging seems limited in the sensitivity of damage that can be measured.

Summary and Conclusions

From the observations made in this study we can draw the following conclusions:

1. Sample preparation is crucial to the success of OIM imaging. Al 2024 samples present special problems for sample preparation while steel samples polish easily. However, the quantitative values obtained can vary widely due to different sample preparation techniques.
2. OIM imaging can detect damage effects easily in steel samples exposed to high blast pressures (e.g., 44 Gpa).
3. The damage observed can be traced through the sample and in general correlates to the strength of the shockwave and the distance of the sample from the blast.
4. The OIM images of low-yield devices that produce low shockwaves (e.g., <7 Gpa) are similar to images obtained from samples that have undergone simple deformation. OIM characterization of this type of explosive damage appears doubtful.
5. The OIM images of high yield devices show extreme damage with a (111) residual texture present. The images from Comp C-4 are especially characteristic and might be used as a fingerprint for damage of this type, although additional work would need to be done to verify this.
6. Failure to obtain data from the Al samples prevented any OIM comparison between blast effects in BCC (steel) versus FCC (Al) crystal structures. Correlation of OIM images with crystal structure and microhardness in samples subjected to explosive blasts would make an interesting future study.

Acknowledgments

This work was funded by the Federal Bureau of Investigation, Dean Federoff, Contract Manager, and performed in part at Ames Laboratory under contract No. W-7405-Eng-82 with the US Department of Energy. The authors would like to thank Rob Tachau and his associates at Sandia National Laboratory for carrying out the dent tests. Special thanks to Paul Cooper for his instruction in explosive forces. Thanks also to Rusty Grey of Los Alamos National Laboratory for helpful discussions concerning shock effects in metals. Our appreciation extends to Dr. Michael A. Smith, Ph.D. for all of his assistance.

References

1. Asay JR, Shahinpoor M, Eds. High-pressure shock compression of solids. New York, NY: Springer-Verlag, 1993.
2. Asay JR, Kerley GI. The response of materials to dynamic loading. Intl J Impact Eng 1987; 5:69–99.
3. Cooper PW. Explosives engineering. Hoboken, NJ: John Wiley and Sons, 1996.
4. Jones OE. Metal response under explosive loading. Behavior and utilization of explosives in engineering design. Proceedings of the 12th annual symposium; 1972 Mar 2–3; University of New Mexico, Albuquerque, NM. Fairfield NJ: Albuquerque American Society of Mechanical Engineers, 1972.
5. Follansbee PS. Metals handbook. 9th ed. Metals Park, OH: ASM International, 1985;198.
6. Carr MJ, Graham RA. Microscopy and microanalysis of shock-processed material. Mic Analysis. San Francisco: San Francisco Press, 1988; 503–8.
7. Gray GT III. Influence of shock loading on the structure/property response of Ti-48Al-2Cr-2Nb and Ti-24Al-11Nb. Jde Phys IV 1994;4: C8-373-78.
8. Follansbee PS, Gray GT III. Dynamic deformation of shock prestrained copper. Mats Sci Eng 1991;A138:23–31.

9. Huang JC, Gray GT III. Substructure evolution and deformation in shock-loaded niobium. Matls Sci Eng 1988;A103:241–55.
10. Gray GT III. Deformation twinning: influence of strain rate. In: Yoo NH, Wuttig M, Eds. Twinning in advanced materials. The minerals, metals, & materials society. Warrendale: TMS, 1984.
11. Gray GT III, Huang JC. Influence of repeated shock loading on the substructure evolution of 99.99 wt% aluminum. Mat Sci Eng 1991;A145:21–35.
12. Hong SI, Gray GT III, Lewandowski JJ. Microstructural evolution in an Al-Zn-Mg-Cu alloy 20 vol% SiC composite shock-loaded to 5 GPA. Scripta Mat 1992;27:431–6.
13. Gray GT III. Deformation substructures induced by high rate deformation. In: Lowe TC, Rollett AD, Follansbee PS, Daehn GS, Eds. Twinning in advanced materials. The minerals, metals, & materials society. Warrendale: TMS,1991;145–58.
14. Dingley DJ, Baba-Kishi KZ, Randle V. Atlas of backscattering kikuchi diffraction patterns. Bristol: IOP Publishing, 1995.

Additional information and reprint request:
L. Scott Chumbley, Ph.D.
Ames Laboratory
214 Wilhelm
Ames, IA 50011